Desalination 503 (2021) 114954

Contents lists available at ScienceDirect

Desalination

journal homepage: www.elsevier.com/locate/desal

A biomimetic antimicrobial surface for membrane fouling control in reverse osmosis for seawater desalination

Miao Tian [a,b,1], HuiJuan Xu [b,1], Lei Yao [c], Rong Wang [b,d,*]

[a] School of Ecology and Environment, Northwestern Polytechnical University, Xi'an 710072, China
[b] Singapore Membrane Technology Centre, Nanyang Environment and Water Research Institute, Nanyang Technological University, 1 Cleantech Loop, Singapore 637141, Singapore
[c] School of Electrical and Information Engineering, Wuhan Institute of Technology, Wuhan 430205, China
[d] School of Civil and Environmental Engineering, Nanyang Technological University, 50 Nanyang Avenue, Singapore 639798, Singapore

HIGHLIGHTS

- A protein-based antimicrobial nanofilm was in-situ fabricated on a commercial SWRO membrane surface.
- The modification did not change the SWRO membrane's selectivity and water permeability.
- The modified membrane demonstrated ~50% bacterial reduction compared to the control membrane.
- The modified membrane had good anti-fouling property applied in SWRO.

GRAPHICAL ABSTRACT

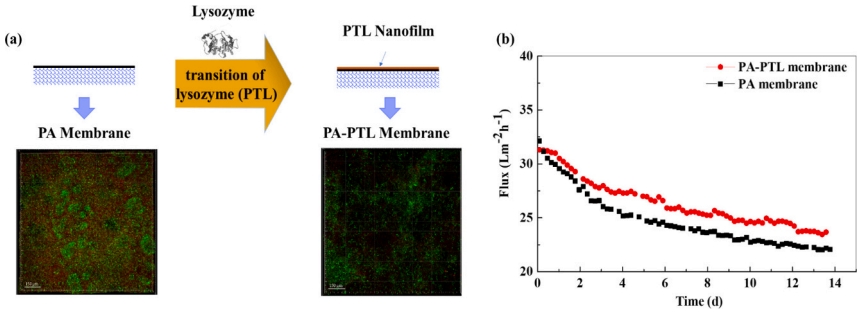

ARTICLE INFO

Keywords:
Reverse osmosis
Antimicrobial
Antifouling
Protein phase transition
Seawater desalination

ABSTRACT

Membrane fouling occurs in all membrane processes. Surface modifications have gained popularity for enhancing membrane antifouling capability via introducing a hydrophilic component or reducing membrane surface roughness. In this work, we proposed to develop a green antimicrobial lysozyme nanofilm on the polyamide membrane surface with remarkable antibacterial and antifouling properties to effectively reduce membrane fouling. The nanofilm is rooted in the molecular assembly of a protein which is an extraction of food and natural products. The nanofilm exhibits the combination of various functions including antimicrobial, antifouling and antibiofilm. This protein-based nanofilm is robustly transferred and self-adhered on the membrane surface by a simple one-step aqueous coating. The modified RO membrane exhibited good performance in bacterial reduction of ~50% in comparison to the control membrane and experienced almost zero loss in water flux and salt rejection under SWRO testing condition. The membrane is further evaluated with real seawater for 14 days and the modified membrane showed its superiority in flux and fouling control which were verified by the confocal laser scanning microscopy (CLSM) and quantified by inductively coupled plasma optical emission spectrometer (ICP-OES). This work demonstrates that the protein-based biomaterials offer a safe and environmentally friendly way of antimicrobials, which can reduce membrane fouling significantly in membrane filtration.

* Corresponding author at: School of Civil and Environmental Engineering, Nanyang Technological University, 639798 Singapore, Singapore.
E-mail address: rwang@ntu.edu.sg (R. Wang).
[1] These authors contributed equally to this work.

https://doi.org/10.1016/j.desal.2021.114954
Received 17 November 2020; Received in revised form 30 December 2020; Accepted 30 December 2020
Available online 22 January 2021
0011-9164/© 2021 Elsevier B.V. All rights reserved.

1. Introduction

Water purification technologies have drawn significant interest owing to water scarcity and environmental related issues. Pressure-driven membrane technologies, such as microfiltration (MF), ultrafiltration (UF), nanofiltration (NF) and reverse osmosis (RO), are attractive due to their low cost, small footprint, high efficiency and less environmental impacts [1–3]. Especially, RO has become a key technology which allows producing clean water from a variety of water resources such as wastewater, brackish water and seawater [3,4]. Thin-film composite (TFC) membrane, generally consisting of a polyamide (PA) separation layer, a polysulfone UF support and nonwoven mechanical support, has been in the RO market for decades due to its excellent separation performance, good chemical resistance and mechanical properties [5–9].

Despite various advantages, TFC membranes still suffer from fouling in practical applications [10]. As a result, the membranes need frequent chemical cleaning, which could eventually shorten the membrane lifespan, increase the operational cost of RO plants (~50% of the total costs) [11]. There are primarily four types of fouling associated with RO membrane: (1) scaling; (2) organic fouling; (3) colloidal fouling; and (4) biofouling. The first three can be significantly reduced through pre-treatment, but biofouling cannot be diminished by pre-treatment as minimal quantity microbial cells can grow, multiply and relocate in the system [12,13].

Many surface modification approaches including but not limited to self-assembly, atom transfer radical polymerization (ATRP), chemical vapour deposition and surface grafting via Ultraviolet (UV) exposure [14] were adopted to introduce antimicrobial materials onto membrane surfaces. Antimicrobial materials can be broadly categorised into two groups [15]: (1) polymers (i.e. zwitterionic polymers, neutral polymers, polyelectrolytes, amphiphilic polymers, quaternary ammonium polymers, biopolymers, hydrophilic polymers, polydopamine [16]); (2) inorganic nanoparticles, such as silver nanoparticles [17,18], titanium dioxide (TiO_2) particles [19], and graphene oxide [14,20]. These antimicrobial/antifouling methods either required tedious synthesis steps, unique facilities, costly chemicals, or had poor coating stability and negative impact on the environment if leaking.

Lysozyme, a natural source of L-Arginine, is harmless and commercially available at low cost. They can be grafted to the polyamide surface via a chemical reaction and shows excellent antifouling property. However, current modification methods may alter the polyamide layer by either increase the membrane resistance or deteriorate the cross-linking structure. The intrinsic permeability and selectivity of these membrane evaluated under brackish water RO (BWRO) condition were slightly reduced and were not even evaluated under high salinity testing condition, such as seawater desalination (SWRO) [21,22]. Chen et al. have constructed a covalently bonded zwitterionic amino acid L-Arginine on the surface of a hand-made BWRO membrane via reacting with the residual acyl chloride groups of the freshly prepared polyamide in one-step chemical reaction [21]. The result revealed that the permeability and antifouling properties of the BWRO membrane were enhanced in the brackish water testing due to the enhanced hydrophilicity. However, this kind of modification needs to react with the freshly prepared polyamide and alter the intrinsic structure of the polyamide layer with a sacrifice in its selectivity and limit its application in SWRO. In another work, a covalently-bonded lysozyme was immobilized on polyamide RO membranes via two-steps chemical reactions. The polyamide was firstly modified with 6-amino caproic acid (ACA) by interfacial polymerization of residue trimesoyl chloride (TMC) and ACA, then lysozyme was immobilized onto the ACA-modified polyamide layer by an amine coupling reaction using 1-ethyl-3-(3-dimethylaminopropyl) carbodiimide (EDC) and N-hydroxysuccinimide (NHS) [22]. However, the flux of aforesaid membrane decreased by about 50% and the salt rejection was maintained 90% of the unmodified membranes using 0.05 wt% NaCl feed solution. By far, there was no report on exploiting the lysozyme in SWRO application properly due to the sacrificed rejection of the current methods.

Recently, Yang's group has reported a novel supramolecular assembled proteinaceous material to convey broad-spectrum antimicrobial properties of medical devices, which shows excellent performance toward both Gram-positive/negative bacteria and fungi [23,24]. The reported phase-transited lysozyme (PTL) nanofilm exhibited a 5-fold higher L-Arginine concentration than that of the native lysozyme and can robustly adhere to any materials or surfaces [25]. The PTL nanofilm surface is constituted of net positive charge and hydrophobic amino acid residues, which synergistically contribute to the antimicrobial capability. As the PTL was a self-induced reaction and will not react with the backbone of the polyamide, we expected that this PTL film can self-assemble on the polyamide layer and will not alter the intrinsic chemical structure to sacrifice its permeability and selectivity.

Inspired by these works, we introduced the antimicrobial PTL nanofilm onto a commercial SWRO membrane surface in one-step reaction, aiming to mitigate the biofouling in SWRO membrane. The as-prepared membrane was characterized comprehensively including the surface chemical structure, hydrophilicity, morphology, roughness and surface charge. Batch filtration studies were designed to examine the intrinsic membrane permeability, selectivity and antimicrobial performance. Moreover, real seawater was used as feed solution to demonstrate the fouling resistance of the modified membranes. Different from the reported methods, the current modification is able to allow the membrane to maintain 100% intrinsic permeability and salt rejection of the virgin membrane. When performing SWRO tests using real seawater collected from a local plant, ~90% normalized flux after 50-hour testing period and ~75% normalized flux at the end of 14-day testing period were obtained. It is expected that this study could provide a facile approach to effectively mitigate RO membrane fouling in seawater desalination.

2. Experimental

2.1. Membrane materials and chemicals

Lysozyme (from hen egg white), tris(2-carboxyethyl) phosphine (TCEP), 2-[4-(2-hydroxyethyl)piperazin-1-yl] ethanesulfonic acid (HEPES) buffer (pH = 7.2– 7.4), glucose, bovine serum albumin (BSA) and calcofluor white were purchased from Sigma. SYTO 63, fluorescein isothiocyanate (FITC), and concanavalin A (Con A) conjugated with tetramethylrhodamine were from Molecular Probes (USA). A commercial SWRO membrane purchased from Hydrodynamics (Nitto SWC6-LD), coded as PA membrane, was used as a reference. Other materials needed for Adenosine triphosphate (ATP) and extracellular polymeric substances (EPS) characterization are described in Sections 2.5 and 2.8, respectively.

2.2. The preparation of PTL coatings on commercial SWRO membrane

The modification protocol was adopted from the literature [23]. In brief, the phase transition buffer of lysozyme was freshly prepared by mixing equal volume of two solutions: lysozyme (2 mg/ml in 10 mM HEPES buffer at pH 7.2) and TCEP buffer (50 mM TCEP in 10 mM HEPES buffer at pH 4.9) [24]. After transferring the freshly prepared mixture onto the surface of a membrane mounted in a frame, it was incubated for 50 min. The phase transition of lysozyme was initiated spontaneously upon the mixing and PTL nanofilm was formed at the membrane surface in a few minutes. Then, the solution was removed from the membrane surface and the modified membrane was cleaned by HEPES buffer to wash away the residues. The modified membrane, coded as PA-PTL membrane, was stored in DI water for further usage.

Table 1
Properties of the raw seawater collected from a local desalination plant.

Parameters	Value
pH	7.8 ± 0.3
Conductivity (mS/cm)	45.9 ± 2.3
TOC (mg/L)	1.36 ± 0.05
Na (mg/L)	9934.4 ± 175.8
Mg (mg/L)	1880.3 ± 38.7
Ca (mg/L)	422.3 ± 9.5

2.3. Characterization of membranes

The surface and cross-sectional morphologies of control and modified membrane were characterized using a field emission scanning electron microscopy (FESEM, JSM7200F, JEOL Asia Pte Ltd, Japan). The dried membranes were coated with platinum by a sputter coater (JEOL JFC-1600) at 20 mA for 40 s before imaging. The membrane surface topography was characterized with an XE 100 atomic force microscopy (AFM, Park Systems, Korea) in non-tapping mode with a scan area of 10.0 μm × 10.0 μm. Each sample was analysed in triplicate to obtain the average root mean square roughness. The in-air water contact angles of membranes were measured using a goniometer (Contact Angle System OCA, Data Physics Instruments GmbH, Singapore). The average values of the contact angles were obtained from 5 replicates.

Membrane surface chemical composition was determined by X-ray photoelectron spectroscopy in a spot area of 300 × 700 μm (XPS, Kratos Analytical, AXIS Supra) with monochromatic Aluminium Kα source ($h\nu$ = 1486.6 eV) radiation source. Survey spectra were obtained in the range of 0–1200 eV, followed by a high-resolution scan of the C 1s, N 1s and O 1s element regions. The binding energy was calibrated by adjusting the C1 peak to 284.6 eV and analysed using ESCApplication software. The zeta potential of the membrane surface in response to pH ranges from 5.85 to 2.5 and 5.85 to 9.5 were measured respectively using a zeta potential analyzer (SurPASS, Anton Paar, Singapore). By doping with a strong base solution (0.1 M NaOH) or acid solution (0.1 M HCl), the pH of the test medium (10 mM NaCl) was adjusted accordingly.

2.4. Confocal laser scanning microscopy (CLSM) characterization

The biofilm on the membrane surface was imaged by a confocal laser scanning microscopy (CLSM, Zeiss, model LSM710). For the cells staining, the membrane was stained with LIVE/DEAD BacLight™ bacterial viability kit (Molecular Probes, L7012) guided by its protocol provided to differentiate the live cells from the dead ones. The EPS staining procedure was conducted according to a reported procedure with minor modifications [26]. Firstly, SYTO 63 (20 μM, 100 μl) was

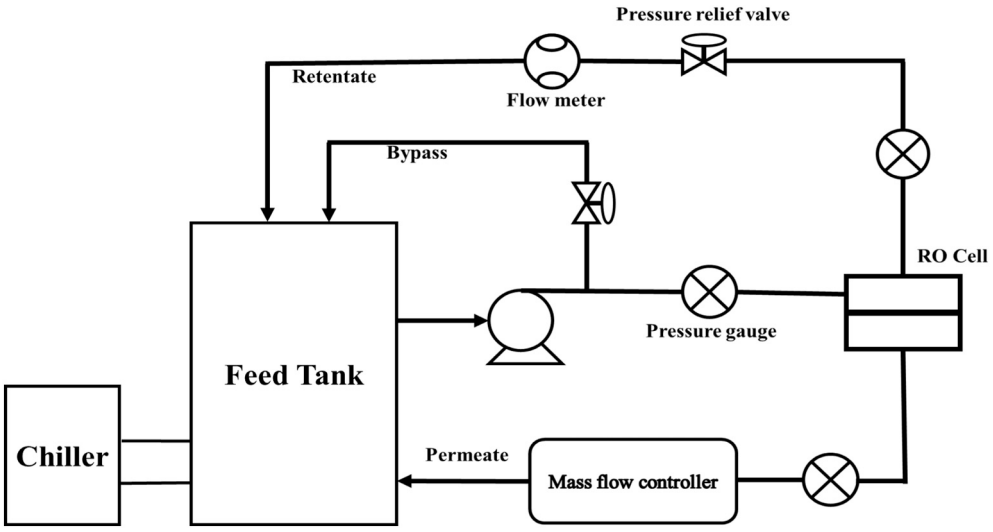

Fig. 1. Schematic diagram of SWRO setup.

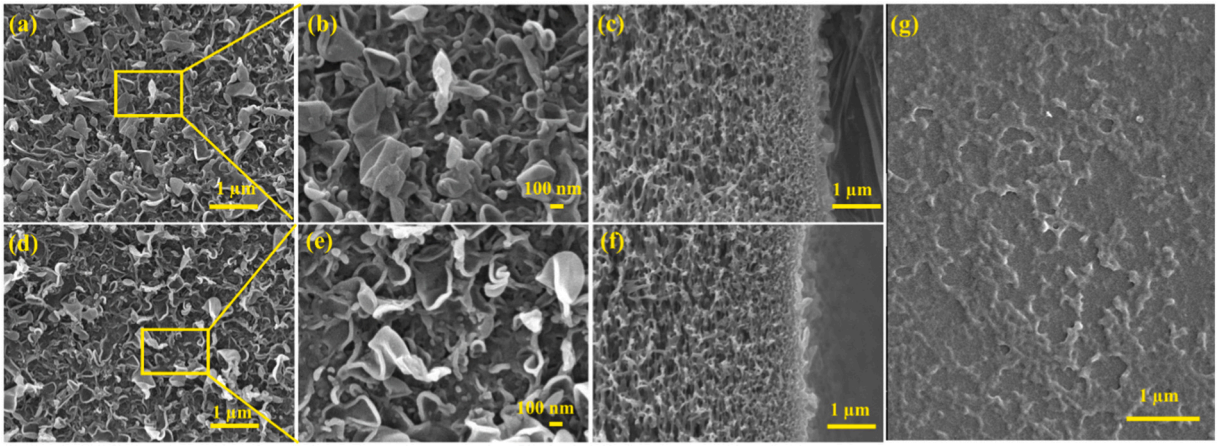

Fig. 2. Surface images of control PA membrane (a and b) and PA-PTL membrane (d and e); cross-sectional images of control PA membrane (c) and PA-PTL membrane (f). Characterization of PTL film on a silicon wafer with an extended reaction time of 2 h was illustrated in (g).

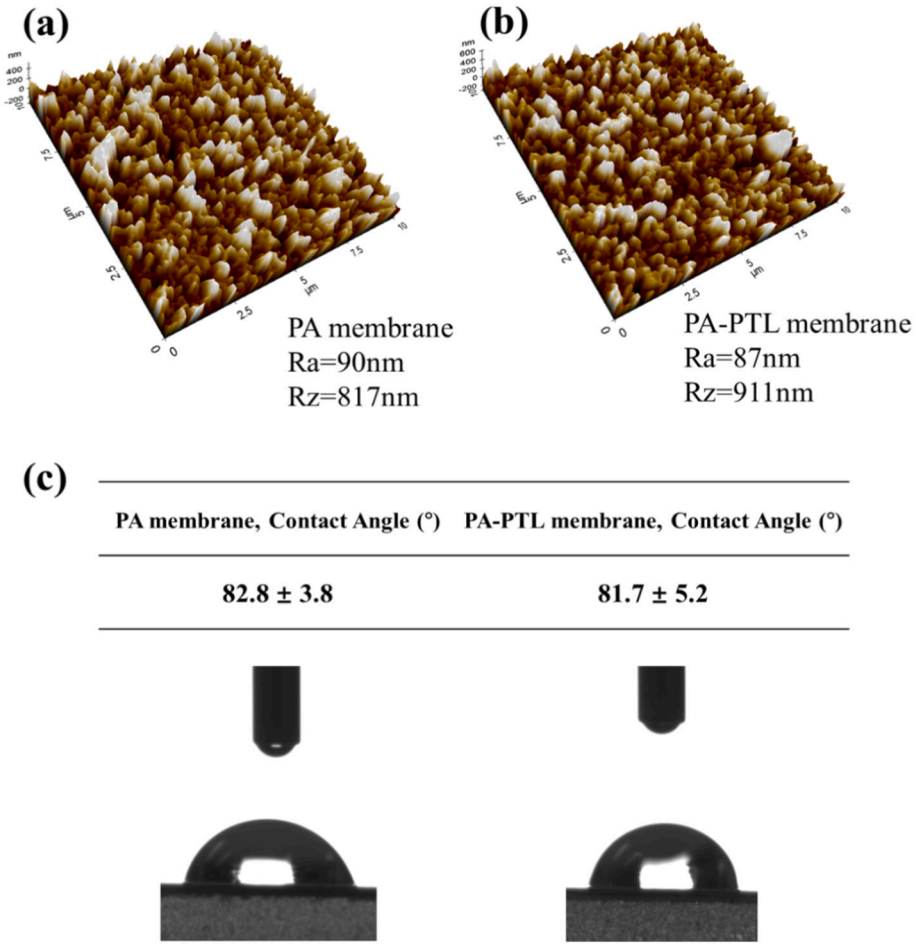

Fig. 3. Surface topography and roughness of the control PA layer (a) and PA-PTL layer (b); static water contact angle (WCA) of control PA membrane and PA-PTL membrane (c).

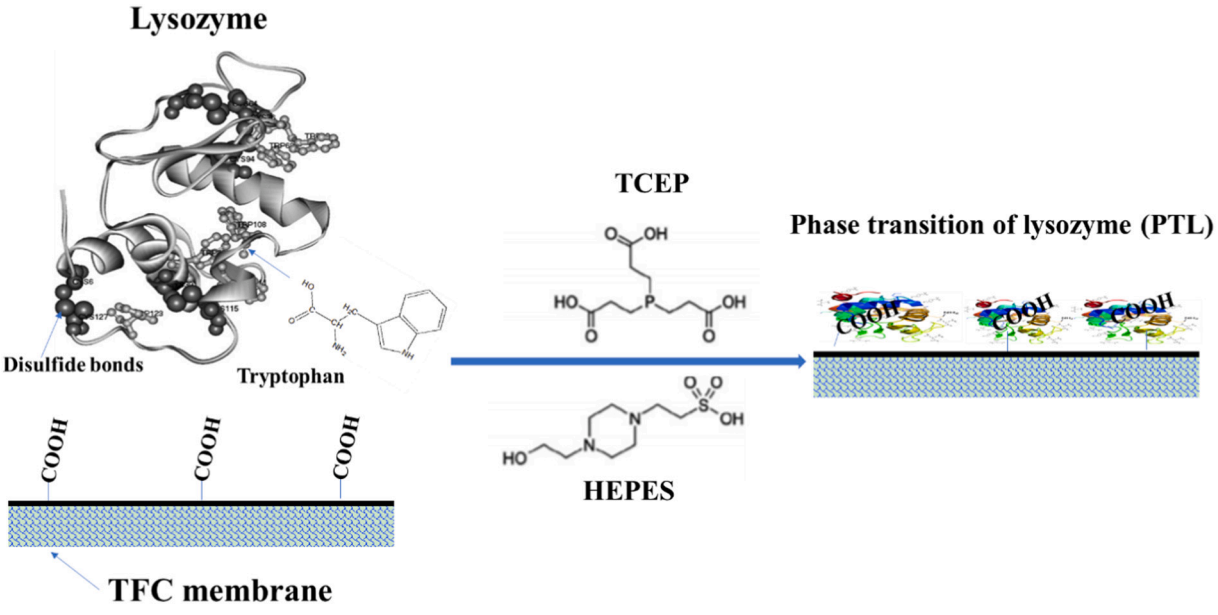

Fig. 4. Schematic of the phase transition of lysozyme and PTL formed on a commercial SWRO membrane surface [34].

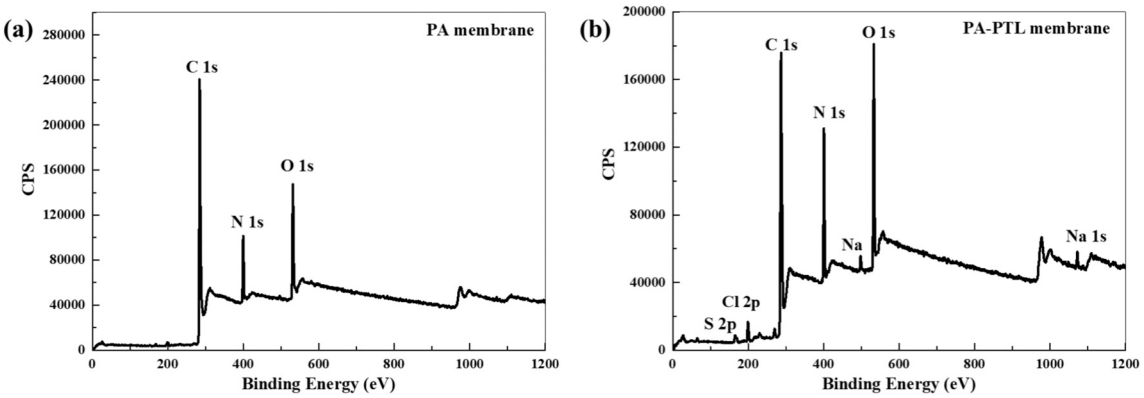

(c)

Sample ID	Atomic concentration (%)			C/N ratio
	C	N	O	
PA membrane	77.6±0.7	9.9±0.6	12.1±0.8	7.84
PA-PTL membrane	68.7±1.3	16.1±0.2	15.3±1.1	4.27

Fig. 5. XPS characterization of prepared membrane surfaces. Survey spectra of the control PA membrane (a) and PA-PTL membrane (b). The atomic concentrations of each membrane are summarized in the table (c).

added to the membrane sample for 20 min to stain the total cells. Secondly, a $NaHCO_3$ buffer (0.1 M, 100 μl) followed by a FITC solution (10 g l^{-1}, 10 μl), was used to stain proteins. The stained membrane was mixed with the FITC solution at room temperature for 1 h. Thirdly, the Con A solution (250 mg/ l, 100 μl) was incubated with the sample for another 20 min to bind with the α-polysaccharides, successively by calcofluor white (fluorescent brightener 28, 300 mg/ l, 100 μl) for 20 min to stain the β-linked D-glucopyranose polysaccharides. After each of the above-mentioned staining steps, the membrane was washed with phosphate-buffered saline (pH 7.2) to remove residue dyes for observation by CLSM under 10× objective. The biovolume ($\mu m^3/\mu m^2$) of biofilm was calculated by IMARIS software (version 7.3.1, Bitplane, Switzerland).

2.5. Antimicrobial test for the control and PTL coated membranes

The antimicrobial effect of the PTL coating was determined using an adapted protocol described elsewhere [27]. Firstly, Gram-negative model bacterial strain *E. coli* K12-MG1655 was cultivated in an LB medium for 16 h at 37 °C, and the bacterial suspension was re-inoculated in a fresh medium and grew to OD600 = 1.0. The test inoculum was diluted to a final concentration of about 10^5 CFU/ml. The control and PTL coated membranes were suspended in the diluted inoculum solutions, respectively. Having been incubated in the aforesaid solution at 37 °C for 24 h on a rotary shaker with a speed of 150 rpm, the number of cells attached on surfaces of the control PA and PA-PTL membranes were measured via ATP bioluminescence test [28]. ATP was quantified by firefly luciferin-luciferase bioluminescence method with the CheckLite HS Assay Kit (Kikkoman Biochemifa Company, Japan) and a Lumitester C-110 (Kikkoman Biochemifa Company, Japan).

2.6. Intrinsic separation properties of the control and modified membrane in SWRO

The membranes were assessed in an SWRO system as described in our previous work [7]. In brief, a membrane coupon mounted in a commercial testing cell (Sterlitech, CF042) was compacted using DI water at an applied pressure of 55 bar for 1 h before the water flux measurement at 50 bar. The water permeability and salt rejection of control and modified membrane were evaluated using monitored seawater (3.5 wt% NaCl solution) at 50 bar.

2.7. SWRO testing using real seawater from a local desalination plant

Bacteria strain *Vibrio* sp. B2 [29] isolated from raw seawater, which was collected from a seawater desalination plant in Singapore, was used as model biofouling bacteria in this study. *Vibrio* sp. B2 was cultivated in fresh marine broth for 24 h at 37 °C with continuous shaking. The composition of the seawater was tabulated in Table 1. The cultured cells were centrifuged at 4000 rpm for 15 min and washed with a phosphate buffered saline (PBS; Life Technologies, CS, USA) two times. The washed culture was added to the real seawater for SWRO fouling test at the concentration of approximately10^3 cells/ml.

The SWRO testing was conducted at 55 bar with a surface velocity of 0.17 m/s for 14 days in a circulated crossflow SWRO testing system as described in Fig. 1 [30]. Real seawater containing model bacteria strain *Vibrio* sp. B2 was utilized as feed water in the SWRO testing system. And the feed solution was maintained at 25 ± 1 °C by a stirrer (IKA, Germany) and a chiller (Polyscience, USA). RO membrane with an effective area 0.0045 m^2 was installed in a stainless-steel RO module. The feed pressure was set at 55 bar during the experiment, and the pressure of the feed and permeate streams were monitored via digital pressure gauge (Ashcroft, USA). During the testing period of 14 days, the retentate and permeate were fully recycled back to the feed tank and the flux was monitored at constant pressure. Since the laboratory scale is different from the full scale in terms of membrane area and fouling time, a longer test time is required to evaluate the efficiency of PTL in further research.

2.8. Membrane autopsy

The fouled membranes were taken out from the RO cell for autopsy analysis after the 14-days SWRO test. In brief, the fouled membrane was cut into pieces in the dimension of 3 cm × 3 cm for further usage. After the foulants on the membrane sample were collected by a sponge rod, it was suspended in 10 ml of DI water, followed by 1-minute bath-sonication, and 1-minute vortex. The foulant solution was dried at 110 °C (total foulant) and then heated to 550 °C, and the mass loss at 550 °C represents the organic composition of the foulant. For the

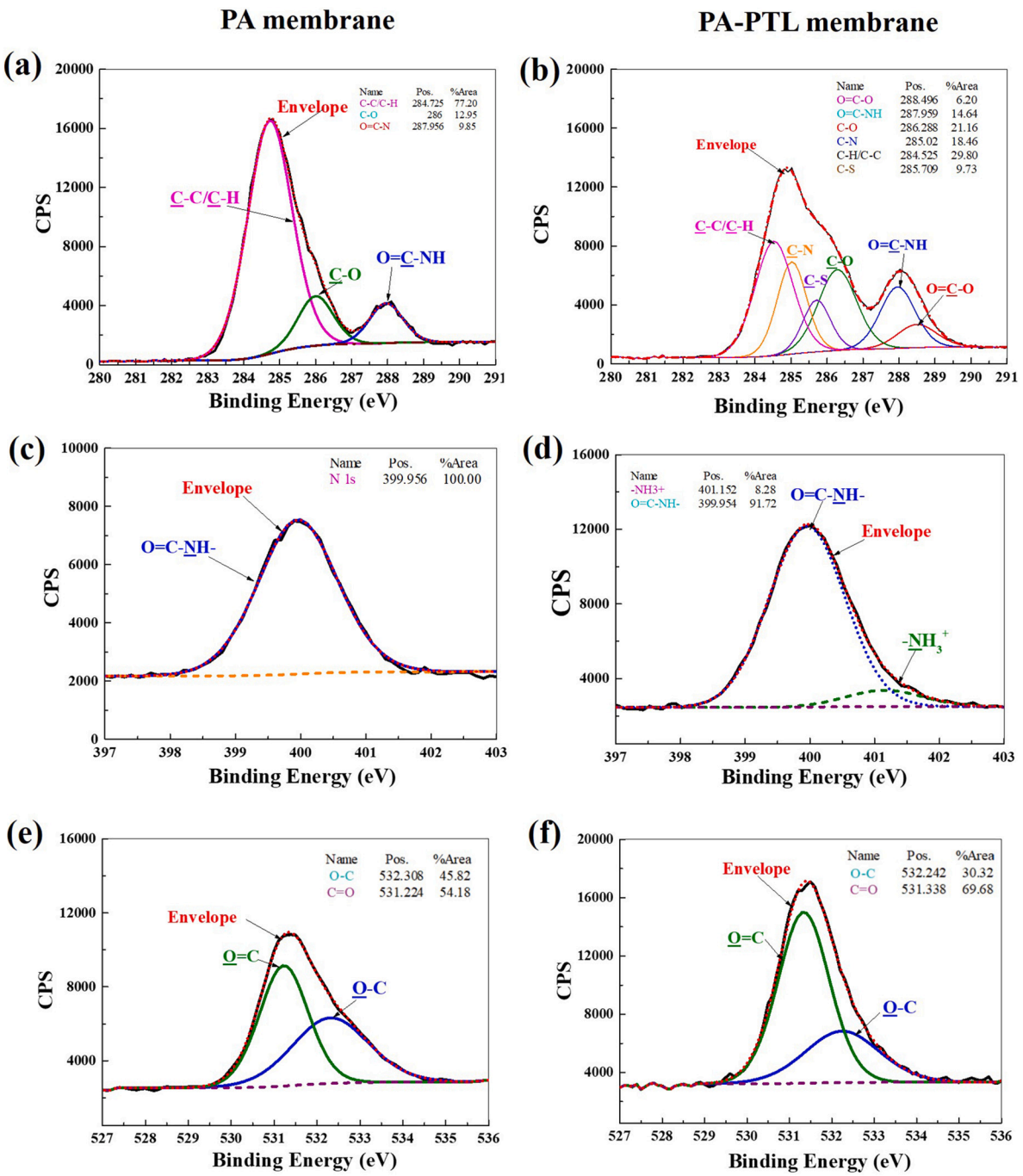

Fig. 6. Deconvolution of C 1s, N 1s and O 1s high-resolution spectra of the prepared membranes, (a) (c) (e) for PA membrane and (b) (d) (f) for PA-PTL membrane. The composition of each component is summarized in the insect tables on the top right of each figure.

inorganic foulant analysis, the foulant detached from membrane surface was digested with 10 ml 2% nitric acid and the inorganic elements in the digested foulant solution were characterized with inductively coupled plasma optical emission spectrometer (ICP-OES, Optima 8000, PerkinElmer, USA).

The amounts of polysaccharides and proteins in the foulant solution were quantified using typical methods described in a previous study [28,31]. In brief, the polysaccharide content was determined by the phenol-sulfuric method using glucose as the calibration standard [32]. The protein amount was determined by the modified Lowry method using a BSA solution as the calibration standard [33].

3. Results and discussion

3.1. Membrane morphology

Fig. 2 presents the surface and cross-sectional morphologies of the control PA and PA-PTL membranes characterized by FESEM in low magnification and high magnification. These images reveal that the two membranes have no significant difference in the surface and cross-section structure, which demonstrates that the PTL coating layer formed in 50 min is very thin and undetectable due to characterization limitation or it follows the pattern of the underneath PA layer. The thickness of PTL formed on a silica wafer in 50 min was confirmed to be less than 30 nm [23]. To understand the morphology of PTL, a PTL

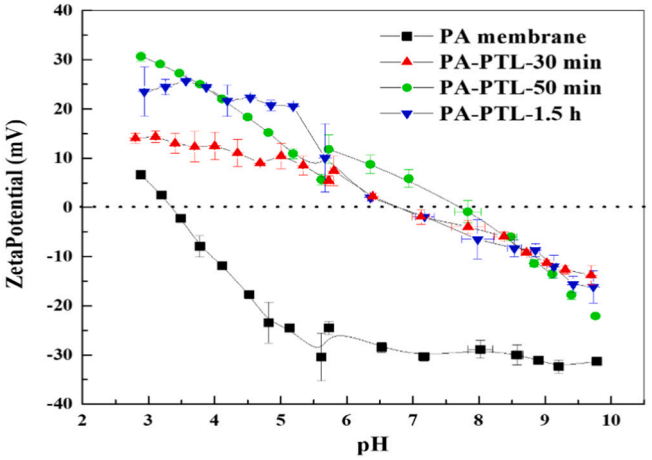

Fig. 7. Zeta potential of the control PA membrane and the modified PA-PTL membranes. The time means the PTL coating time.

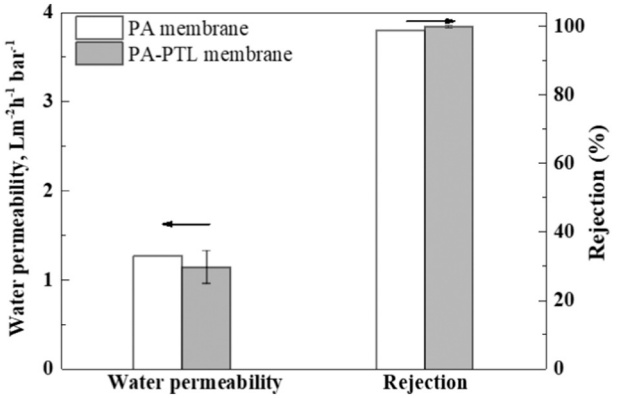

Fig. 8. Pure water permeability and NaCl rejection of the PA and PA-PTL membranes using synthetic seawater (3.5 wt% NaCl solution) at the pressure of 50 bar with a cross velocity of ~0. 08 m/s.

modification was conducted on a silica wafer in an extended time for 2 h and the FESEM image is shown in Fig. 2(g). The reaction time was fixed at 50 min, which is expected to have a minimal effect on the water permeability of the RO membrane, as the PTL film was confirmed to be waterproof in previous work [23].

It is commonly recognized that the surface roughness and hydrophilicity of the TFC membrane are the key properties that significantly influence the membrane's fouling tendency. Thus, we examined the surface 3D topography of control PA and PA-PTL membranes by AFM and the results are presented in Fig. 3(a)–(b). The quantitative analysis of the surface roughness is summarized beneath the 3D image. The roughness average (Ra) and mean roughness depth (Rz) of the control PA membrane are 90 nm and 817 nm, respectively, whereas those of the PA-PTL membrane are 87 nm and 911 nm, respectively. The in-air static water contact angle was used to characterize the surface wettability of the PA and PA-PTL membranes. As shown in Fig. 3(c), both membranes show a similar water contact angle which indicates that the PA and PA-PTL membrane have similar hydrophilicity. The above results further confirm the marginal impact of the PTL coating layer on the surface topography, roughness and hydrophilicity of the pristine PA layer, owing to the ultrathin thickness of PTL and similar physical structure of PA and PTL.

3.2. Chemical compositions of membrane surface

As shown in Fig. 4, lysozyme contains four pairs of disulfide bonds and six tryptophan residues within the globular protein [34]. The modification mechanism of this system is that the specific binding of piperazine ring in HEPES, carboxyl group in TCEP and polyamide onto lysozyme opens the disulfide bonds in lysozyme and converts it into an amyloid substance that can adhere to any substrate surface [24].

It is difficult to differentiate the ultrathin PTL layer from PA by FESEM. Thus X-ray photoelectron spectroscopy (XPS) analysis was utilized to quantify the chemical components of the membrane surface. As illustrated in Fig. 5, the PA-PTL wide scan reveals more signals such as S 2p and Cl 2p, reflecting the existence of a variety of functional groups on the film surface. The constituent elements of the PA and PTL are carbon, nitrogen, and oxygen, with the characteristic binding energy of 284.5 eV for C 1s, 397.9 eV for N 1s, 531.6 eV for O 1s, respectively. As reflected by the C/N atomic ratio, the PA and PTL have a C/N ratio of 7.84 and 4.27, respectively. The C/N ratio of PTL is in the typical range of the PTL nanofilm coated on a variety of substrates, which is consistent with the ratio of native lysozyme. The nanofilm has a higher nitrogen ratio which is due to the existence of amide, amine, and guanidyl groups in amino acids of lysozyme [23].

XPS high-resolution scans of C 1s, N 1s and O 1s further confirm the chemical structure of PTL, which is presented in Fig. 6. As shown in Fig. 6(a), the C 1s spectra of PA is fitted to be C-C/C-H, C—O and O=C-N, which are core components in polyamide of the RO membrane. In contrast, the deconvolution of C1s peak in Fig. 6(b) indicates that the PTL nanofilm is composed of functional groups including aliphatic carbon (C-H/C-C), amines (C—N), thiols (C—S), hydroxyls (C—O), amides (O=C-N) and carboxyl groups (O=C-O) at the peak of 284.6 eV, 285 eV, 285.7 eV, 286.1 eV, 287.9 eV and 288.5 eV, respectively. In Fig. 6(c), only O=C-NH- was detected in PA, whereas in Fig. 6(d), two deconvoluted peaks for N element was found in PTL. The two peaks at 399.9 eV and 401.2 eV belong to O=C-NH- and, and -NH_3^+ group. As shown in Fig. 6(e)–(f), the spectra of O element in PA and PTL were also

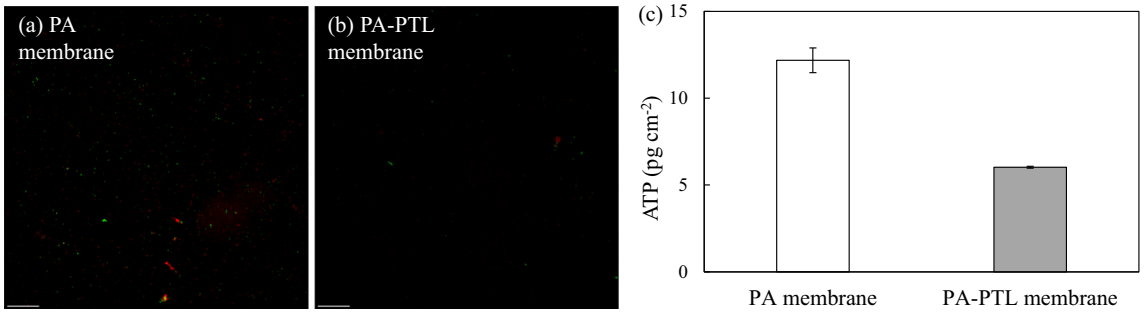

Fig. 9. CLSM images of attached microorganisms on the control PA membrane (a) and the modified PA-PTL membrane (b). (Live cells in green; dead cells in red.) (c) Attachment of microorganisms quantified based on ATP. (For interpretation of the references to color in this figure legend, the reader is referred to the web version of this article.)

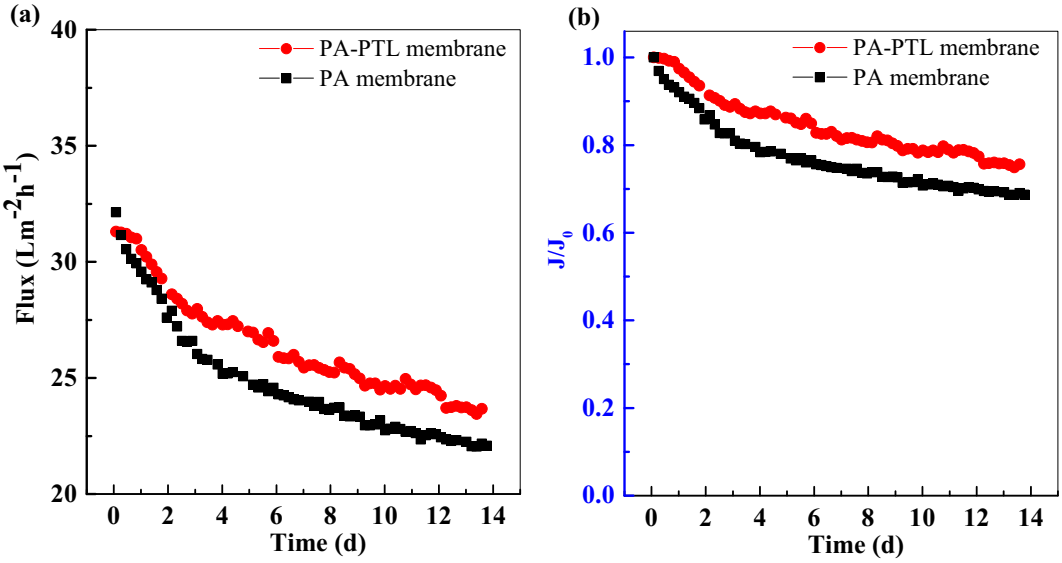

Fig. 10. Water flux (a) and normalized water flux (b) decline profiles of the control membrane (PA) and modified membrane (PA-PTL) in a 14-day RO test (raw seawater, at 55 bar operating pressure).

deconvoluted into two peaks at 531.3 eV (O=C) and 532.3 eV (O-C). As demonstrated above, the PTL nanofilm with different chemical components was successfully fabricated on the PA surface of a commercial TFC RO membrane.

3.3. Membrane surface charge and intrinsic permeability

Surface charge, recognized as an essential performance index of a RO membrane, is well known to play a role in membrane fouling. The surface charge of control PA and PA-PTL membranes with varied coating time in response to pH from 3 to 9.5 are shown in Fig. 7. The iso-electric point (IEP) of the PA and PA-PTL membranes are pH = ~3.5 and pH = ~7, respectively. In most RO operation system, the pH of the feed solution was regulated in the range from 6 to 8 [35,36]. Generally, in the pH range of 6– 8, the PA membrane with a functional group -COOH shows a significant negative charge (~− 30 mV), while the PA-PTL membrane shows neutral or a slightly positive charge (−5– 2 mV). The positive charge of the PA-PTL membrane is attributed to the existence of -NH_3^+ group in PTL layer which has been evidenced by the XPS characterization in Fig. 6(d). When pH is above the IEP, the coating time shows no significant impact on the surface charge; while below the IEP, the surface charge is more intense with an extended coating time.

The PTL layer was reported to be slightly waterproof [23], which we speculated may adversely reduce the intrinsic permeability of the control TFC membrane. Thus, the effect of PTL layer on the intrinsic permeability and salt rejection of the control membrane was examined, and the results are elaborated in Fig. 8. The results show that the PTL layer slightly reduces the pure water permeability and have no significant impact on salt rejection under the seawater testing condition. The results suggest that PTL coating may be an excellent antifouling modification method to enhance the antifouling or antimicrobial properties, as it does not sacrifice the membrane's intrinsic permeability.

3.4. Antimicrobial test of the membranes

The amount of the microorganisms attached on the control and PTL modified membrane surfaces was evaluated using the CLSM and ATP analysis. The high-resolution CLSM images shown in Fig. 9 indicate that there are less living and dead cells on the surface of the PA-PTL membrane. The ATP test quantified the microorganisms on the membranes surface and further confirms that the amount of microorganism on PTL modified membranes is 49.4% of those on the commercial RO membrane. The enhanced antimicrobial properties of the PA-PTL membrane could be attributed to the antimicrobial lysozyme in the PTL film, as lysozyme has an on-lytic mechanism targeting the cell wall, which leads to bacterial autolysis [37,38].

3.5. SWRO testing using real seawater

The control and modified membranes were further evaluated in the SWRO system using real seawater. The water flux and normalized water flux decline profiles of the PA and modified PA-PTL are presented in Fig. 10. It was observed that the modified PA-PTL membrane showed a considerable higher water flux as compared with those of the control membrane during the whole testing period of 14 days. At a constant feed pressure of 55 bar, the flux of the control membrane decreased from 32.1 LMH to 22.0 LMH after the 14-day operation, with the average flux decrease rate at 0.721 LMH/day. However, due to the PTL coating, the average flux decrease of the modified PA-PTL was around 0.564 LMH/day, which is 21.8% less flux drop compared to the control membrane. This implied that the PA-PTL membrane has a better anti-fouling performance compared to the control membrane applied in seawater desalination.

To identify the anti-fouling property of modified PA-PTL membrane, the surface morphologies of the fouled membranes were characterized by CLSM. As shown in Fig. 11(a–b), the CLSM images of cells show that the surface of both control and modified PA-PTL membranes were occupied with dead and live cells after 14-day SWRO testing. The control RO membrane was occupied by a dense and thick layer of cells. In contrast, the biofilm structure on the PA-PTL membrane was loose, and fewer cells were observed on the PA-PTL membrane surface. Furthermore, the CLSM images of EPS in Fig. 11(c–d) reveal that less EPS were deposited on the modified PA-PTL membrane in comparison to the control PA membrane. The quantified biovolumes shown in Fig. 11(e) of live cells, dead cells and total cells in the modified PA-PTL membrane agree well with CLSM images. For instance, the biovolume of the total cells on the PA membrane was 4.34 $\mu m^3/\mu m^2$, while 1.82 $\mu m^3/\mu m^2$ on the PA-PTL membrane surface, indicating 58.1% reduction due to lysozyme-based coating. Due to the unique function of lysozyme in which it attacks peptidoglycans in the cell walls of bacteria and causes cell lysis [37], the most significant reduction was observed on total cells stained by SYTO 63 in Fig. 11(f), which subsequently resulted in the EPS

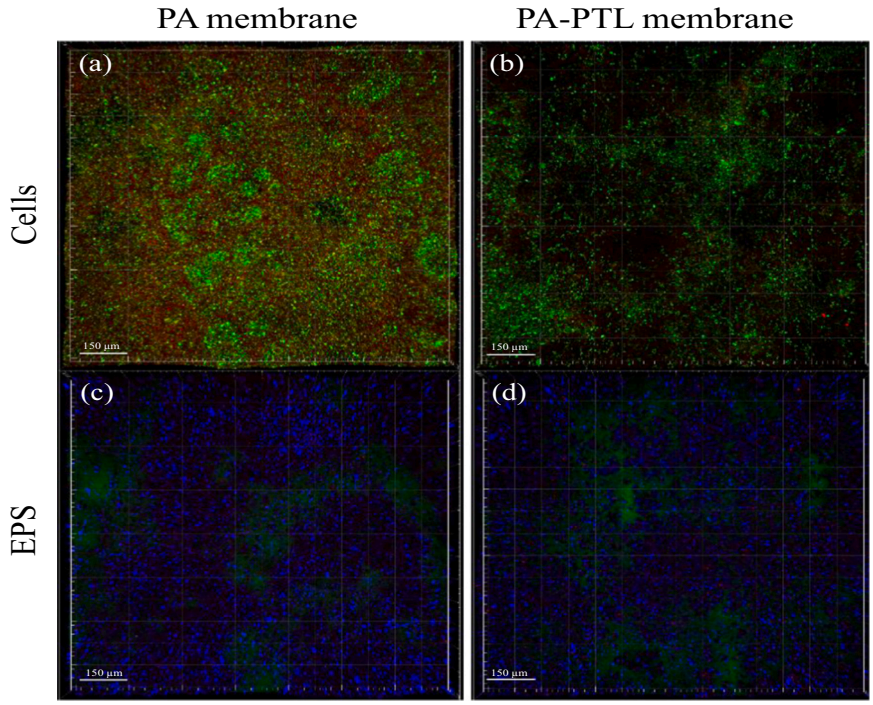

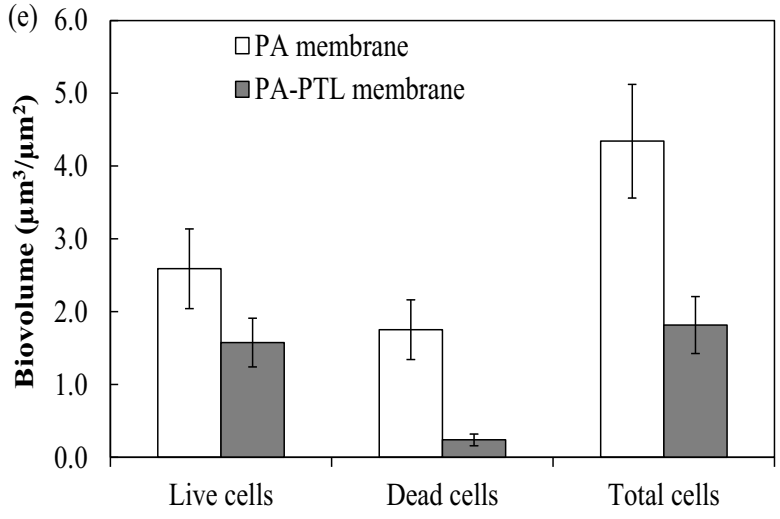

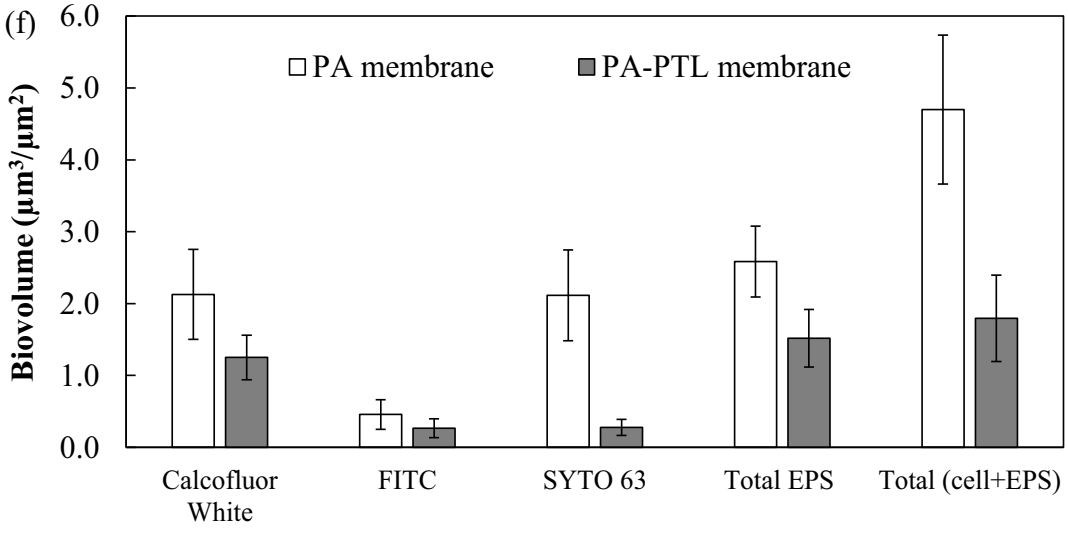

(caption on next page)

Fig. 11. Surface characterization of the membranes after 14-days RO testing. (a) and (b) represent the CLSM images of live/dead cells (live cells in green; dead cells in red) of control PA and modified PA-PTL membrane, respectively; while (c) and (d) represent the CLSM images of proteins and polysaccharide (PS) of control PA and modified PA-PTL membrane, respectively (α-PS, yellow; β-PS, blue; protein, green; total cells, red); (e) the quantified biovolumes of live cells, dead cells and total cells in the control PA and modified PA-PTL membrane (n = 8); (f) The quantified biovolumes of EPS of control PA and modified PA-PTL membrane. (α-PS (ConA); β-PS (Calcofluor white); protein (FITC); bacterial cells (SYTO 63); n = 8).

Table 2
Foulant composition on the membrane surface determined by EPS analysis, ATP and ICP-OES.

	PA membrane (control)	PA-PTL membrane (modified)
Total foulant (μg/cm^2)	456.1 ± 34.1	263.2 ± 24.8
Organic foulant/total foulant (%)	77.8	80.3
Proteins (μg/cm^2)	17.48 ± 0.32	6.44 ± 0.21
Polysaccharides (μg/cm^2)	20.99 ± 1.29	13.75 ± 1.98
ATP (ng/cm^2)	11.89 ± 0.71	2.06 ± 0.15
Ca (μg/cm^2)	11.76 ± 0.52	10.35 ± 0.15
Mg (μg/cm^2)	6.69 ± 0.23	4.30 ± 0.07
Na (μg/cm^2)	42.84 ± 2.05	42.49 ± 1.68
Fe (μg/cm^2)	1.88 ± 0.08	2.49 ± 0.23
P (μg/cm^2)	0.67 ± 0.03	0.42 ± 0.02
Si (μg/cm^2)	0.14 ± 0.01	0.24 ± 0.01
S (μg/cm^2)	8.31 ± 0.12	4.33 ± 0.08

reduction due to less live cells proliferation. These results indicate that the developed membrane surface modification method effectively mitigated membrane fouling in practical SWRO process.

Foulant composition on the membrane surface was also quantitated by EPS analysis, ATP and ICP-OES and results are summarized in Table 2. These results are consistent with the CLSM and SEM images. For instance, the total foulant on the PA-PTL membrane was 0.263 mg/cm^2, which decreased by 42.3% compared to foulants on the PA membrane (0.456 mg/cm^2). The organic fouling was the major contributor for both RO membranes as the contents of organic component account for about 77.8% and 80.3% of the dry foulants, respectively. Also, there was no significant difference for inorganic foulant on the membrane surface, especially Na content (both around 42 μg/cm^2). This is due to that the PTL layer did not affect the salt rejection of the RO membrane. Furthermore, the EPS such as polysaccharides and proteins on the modified membrane also decreased significantly. For proteins, it decreased from 17.48 μg/cm^2 to 6.44 μg/cm^2, indicating 63.1% reduction. For polysaccharides, it decreased by only 34.5%, which was less significant compared to protein reduction (63.1%). This implied that PTL was more effective to inhibit protein secretion of microorganisms and subsequent their attachment onto the membrane surface.

The ATP was also determined to quantify the active bacteria in the RO foulants, which was associated closely with membrane biofouling. It shows that the ATP content on modified RO membrane was only 17.3% compared to that of the control membrane, indicating an 81.7% reduction. In other words, the lysozyme on the PA-PTL membrane highly prevented the proliferation of deposited cells on the membrane surface. This is consistent with the enzymatic activity of lysozyme from PTL. By autopsy analysis, it further confirms that the coated lysozyme layer effectively mitigated membrane biofouling and organic fouling. Evidenced by both the short-term attachment assay and 14-days SWRO experiment, the PA-PTL coating not only inhibited the bacterial attachment to the modified membrane but also reduced the biofilm formation on the membrane surface.

Membrane fouling is very complicated and is closely related to membrane material, module design, fluid dynamic condition, and operation duration, etc. Although the current results from approximately 14-day lab-scale feasibility study are promising, it may be hasty to conclude their efficiency in fouling control in long-term full-scale operation in years. The biofilm formation on membrane surface is normally initiated with protein or bacterial cell attachment to the membrane, which was effectively mitigated by the PTL nanofilm shown in current study. However, it is uncertain that the PTL nanofilm could effectively control the long-term biofouling behaviour in practical operation [39]. Firstly, a low adhesion during the initial stage may have limited effect on ultimately very long biofilm growth [40]. A typical laboratory-scale fouling experiments (young biofilms developed on the membrane) cannot represent full-scale conditions. Secondly, the constant nutrient supply provided by the feed water, which is different under two situations of short-term laboratory and long-term practical operations, is more beneficial for long-term biofilm growth and biofouling than in the short-term test. Therefore, it is necessary to further study the PTL nanofilm in fouling control in long-term pilot or full-scale operation.

4. Conclusions

In this work, an antimicrobial lysozyme nanofilm was developed based on a supramolecular assembly of a protein in one-step reaction on a commercial RO membrane, aiming to mitigate membrane fouling in the SWRO system. The modified RO membrane exhibited ~50% bacterial reduction in comparison to the control membrane and experienced almost zero loss in water flux and salt rejection under RO testing condition. The modified membrane excelled the control membrane in terms of flux in a 14-day SWRO test using real seawater from a local RO plant. Through qualitative and quantitative analysis methods, the modified membrane demonstrated better anti-fouling property as the lysozyme nanofilm can inhibit the microbial growth and EPS production on the membrane surface. This work proved that the protein-based biomaterials can offer a safe and environmentally friendly solution to antimicrobial membrane surface modification, which can significantly reduce membrane fouling in an SWRO system. Since the membrane fouling is challenging and complicated in full-scale long-term operation, the anti-fouling performance of the PTL nanofilm should be further demonstrated in pilot or full scale SWRO systems.

CRediT authorship contribution statement

Miao Tian and HuiJuan Xu: Investigation, Data curation, Writing - Original draft
Lei Yao: Writing - Review & editing
Rong Wang: Supervision, Writing - Review & editing, Project administration, Funding acquisition.

Declaration of competing interest

The authors declare that they have no known competing financial interests or personal relationships that could have appeared to influence the work reported in this paper.

Acknowledgements

We acknowledge funding support from Northwestern Polytechnical University (China), Hubei Provincial Department of Education (B2020052) and the Singapore Economic Development Board to the Singapore Membrane Technology Centre (SMTC), Nanyang Environment and Water Research Institute, Nanyang Technological University.

References

[1] C. Tristán, M. Fallanza, R. Ibáñez, I. Ortiz, Recovery of salinity gradient energy in desalination plants by reverse electrodialysis, Desalination. 496 (2020) 114699, https://doi.org/10.1016/j.desal.2020.114699.

[2] J. Zhang, G. Weston, X. Yang, S. Gray, M. Duke, Removal of herbicide 2-methyl-4-chlorophenoxyacetic acid (MCPA) from saline industrial wastewater by reverse osmosis and nanofiltration, Desalination. 496 (2020) 114691, https://doi.org/10.1016/j.desal.2020.114691.

[3] C.D. Peters, N.P. Hankins, The synergy between osmotically assisted reverse osmosis (OARO) and the use of thermo-responsive draw solutions for energy efficient, zero-liquid discharge desalination, Desalination. 493 (2020) 114630, https://doi.org/10.1016/j.desal.2020.114630.

[4] D.M. Davenport, A. Deshmukh, J.R. Werber, M. Elimelech, High-pressure reverse osmosis for energy-efficient hypersaline brine desalination: current status, design considerations, and research needs, Environ. Sci. Technol. Lett. 5 (2018) 467–475, https://doi.org/10.1021/acs.estlett.8b00274.

[5] T. Matsuura, Progress in membrane scince and technology for seawater desalination - a review, Desalination. 134 (2001) 47–54, https://doi.org/10.1016/S0011-9164(01)00114-X.

[6] Y. Zhao, Z. Zhang, L. Dai, H. Mao, S. Zhang, Enhanced both water flux and salt rejection of reverse osmosis membrane through combining isophthaloyl dichloride with biphenyl tetraacyl chloride as organic phase monomer for seawater desalination, J. Memb. Sci. 522 (2017) 175–182, https://doi.org/10.1016/j.memsci.2016.09.022.

[7] Y. Li, S. Qi, M. Tian, W. Widjajanti, R. Wang, Fabrication of aquaporin-based biomimetic membrane for seawater desalination, Desalination. 467 (2019) 103–112, https://doi.org/10.1016/j.desal.2019.06.005.

[8] C.Y. Tang, Y.N. Kwon, J.O. Leckie, Probing the nano- and micro-scales of reverse osmosis membranes-a comprehensive characterization of physiochemical properties of uncoated and coated membranes by XPS, TEM, ATR-FTIR, and streaming potential measurements, J. Memb. Sci. 287 (2007) 146–156, https://doi.org/10.1016/j.memsci.2006.10.038.

[9] C. Fang, F. Lv, D. Huang, J. Su, Coupling transport of water and ions through a carbon nanotube: a novel desalination phenomenon induced by tuning the pressure direction, Desalination. 492 (2020) 114656, https://doi.org/10.1016/j.desal.2020.114656.

[10] G. Dong Kang, Y. Ming Cao, Development of antifouling reverse osmosis membranes for water treatment: a review, Water Res. 46 (2012) 584–600. doi: https://doi.org/10.1016/j.watres.2011.11.041.

[11] A. Matin, Z. Khan, S.M.J. Zaidi, M.C. Boyce, Biofouling in reverse osmosis membranes for seawater desalination: phenomena and prevention, Desalination. 281 (2011) 1–16, https://doi.org/10.1016/j.desal.2011.06.063.

[12] M. Herzberg, M. Elimelech, Biofouling of reverse osmosis membranes: role of biofilm-enhanced osmotic pressure, J. Memb. Sci. 295 (2007) 11–20, https://doi.org/10.1016/j.memsci.2007.02.024.

[13] R.S. Hebbar, A.M. Isloor, K. Ananda, A.F. Ismail, Fabrication of polydopamine functionalized halloysite nanotube/polyetherimide membranes for heavy metal removal, J. Mater. Chem. A 4 (2016) 764–774, https://doi.org/10.1039/c5ta09281g.

[14] X. Huang, K.L. Marsh, B.T. McVerry, E.M.V. Hoek, R.B. Kaner, Low-fouling antibacterial reverse osmosis membranes via surface grafting of graphene oxide, ACS Appl. Mater. Interfaces 8 (2016) 14334–14338, https://doi.org/10.1021/acsami.6b05293.

[15] R.R. Choudhury, J.M. Gohil, S. Mohanty, S.K. Nayak, Antifouling, fouling release and antimicrobial materials for surface modification of reverse osmosis and nanofiltration membranes, J. Mater. Chem. A 6 (2018) 313–333, https://doi.org/10.1039/c7ta08627j.

[16] Y. Xu, D. Guo, T. Li, Y. Xiao, L. Shen, R. Li, Y. Jiao, H. Lin, Manipulating the mussel-inspired co-deposition of tannic acid and amine for fabrication of nanofiltration membranes with an enhanced separation performance, J. Colloid Interface Sci. 565 (2020) 23–34, https://doi.org/10.1016/j.jcis.2020.01.004.

[17] Z. Liu, L. Qi, X. An, C. Liu, Y. Hu, Surface engineering of thin film composite polyamide membranes with silver nanoparticles through layer-by-layer interfacial polymerization for antibacterial properties, ACS Appl. Mater. Interfaces 9 (2017) 40987–40997, https://doi.org/10.1021/acsami.7b12314.

[18] M. Ben-Sasson, X. Lu, E. Bar-Zeev, K.R. Zodrow, S. Nejati, G. Qi, E.P. Giannelis, M. Elimelech, In situ formation of silver nanoparticles on thin-film composite reverse osmosis membranes for biofouling mitigation, Water Res. 62 (2014) 260–270, https://doi.org/10.1016/j.watres.2014.05.049.

[19] S.Y. Kwak, S.H. Kim, S.S. Kim, Hybrid organic/inorganic reverse osmosis (RO) membrane for bactericidal anti-fouling. 1. Preparation and characterization of TiO2 nanoparticle self-assembled aromatic polyamide thin-film-composite (TFC) membrane, Environ. Sci. Technol. 35 (2001) 2388–2394. doi:https://doi.org/10.1021/es0017099.

[20] H.J. Kim, Y.S. Choi, M.Y. Lim, K.H. Jung, D.G. Kim, J.J. Kim, H. Kang, J.C. Lee, Reverse osmosis nanocomposite membranes containing graphene oxides coated by tannic acid with chlorine-tolerant and antimicrobial properties, J. Memb. Sci. 514 (2016) 25–34, https://doi.org/10.1016/j.memsci.2016.04.026.

[21] D. Chen, T. Liu, J. Kang, R. Xu, Y. Cao, M. Xiang, Enhancing the permeability and antifouling properties of polyamide composite reverse osmosis membrane by surface modification with zwitterionic amino acid l-arginine, Adv. Mater. Interfaces 1900706 (2019) 1–8, https://doi.org/10.1002/admi.201900706.

[22] D. Saeki, S. Nagao, I. Sawada, Y. Ohmukai, T. Maruyama, H. Matsuyama, Development of antibacterial polyamide reverse osmosis membrane modified with a covalently immobilized enzyme, J. Memb. Sci. 428 (2013) 403–409. doi:doi:https://doi.org/10.1016/j.memsci.2012.10.038.

[23] D. Wang, Y. Ha, J. Gu, Q. Li, L. Zhang, P. Yang, 2D protein supramolecular nanofilm with exceptionally large area and emergent functions, Adv. Mater. 28 (2016) 7414–7423, https://doi.org/10.1002/adma.201506476.

[24] F. Yang, F. Tao, C. Li, L. Gao, P. Yang, Self-assembled membrane composed of amyloid-like proteins for efficient size-selective molecular separation and dialysis, Nat. Commun. 9 (2018). doi:https://doi.org/10.1038/s41467-018-07888-2.

[25] J. Gu, Y. Su, P. Liu, P. Li, P. Yang, An environmentally benign antimicrobial coating based on a protein supramolecular assembly, ACS Appl. Mater. Interfaces 9 (2017) 198–210, https://doi.org/10.1021/acsami.6b13552.

[26] M.Y. Chen, D.J. Lee, J.H. Tay, K.Y. Show, Staining of extracellular polymeric substances and cells in bioaggregates, Appl. Microbiol. Biotechnol. 75 (2007) 467–474, https://doi.org/10.1007/s00253-006-0816-5.

[27] H. Xu, Y. Liu, Control and cleaning of membrane biofouling by energy uncoupling and cellular communication, Environ. Sci. Technol. 45 (2011) 595–601, https://doi.org/10.1021/es102911m.

[28] H. Xu, Y. Liu, D-amino acid mitigated membrane biofouling and promoted biofilm detachment, J. Memb. Sci. 376 (2011) 266–274, https://doi.org/10.1016/j.memsci.2011.04.030.

[29] L.H. Kim, T.H. Chong, Physiological responses of salinity-stressed Vibrio sp. and the effect on the biofilm formation on a nanofiltration membrane, Environ. Sci. Technol. 51 (2017) 1249–1258. doi:https://doi.org/10.1021/acs.est.6b02904.

[30] W. Yin, J.S. Ho, E.R. Cornelissen, T.H. Chong, Impact of isolated dissolved organic fractions from seawater on biofouling in reverse osmosis (RO) desalination process, Water Res. 168 (2020) 115198, https://doi.org/10.1016/j.watres.2019.115198.

[31] R. Wang, D. Liang, X. Liu, W. Fan, S. Meng, W. Cai, Effect of magnesium ion on polysaccharide fouling, Chem. Eng. J. 379 (2020) 122351, https://doi.org/10.1016/j.cej.2019.122351.

[32] M. Dubois, K.A. Gilles, J.K. Hamilton, P.A. Rebers, F. Smith, Colorimetric method for determination of sugars and related substances, Anal. Chem. 28 (1956) 350–356, https://doi.org/10.1021/ac60111a017.

[33] O.H. Lowry, N.J. Rosebrough, A.L. Farr, R.J. Randall, Protein measurement with the Folin phenol reagent, J. Biol. Chem. 193 (1951) 265–275, https://doi.org/10.1016/0922-338X(96)89160-4.

[34] L.Z. Wu, Y.B. Sheng, J. Bin Xie, W. Wang, Photoexcitation of tryptophan groups induced reduction of disulfide bonds in hen egg white lysozyme, J. Mol. Struct. 882 (2008) 101–106, https://doi.org/10.1016/j.molstruc.2007.09.016.

[35] A. Farhat, F. Ahmad, N. Hilal, H.A. Arafat, Boron removal in new generation reverse osmosis (RO) membranes using two-pass RO without pH adjustment, Desalination. 310 (2013) 50–59. doi:doi:https://doi.org/10.1016/j.desal.2012.10.003.

[36] J. Redondo, M. Busch, J.P. De Witte, Boron removal from seawater using FILMTECTM high rejection SWRO membranes, Desalination. 156 (2003) 229–238, https://doi.org/10.1016/S0011-9164(03)00345-X.

[37] J. Humann, L.L. Lenz, Bacterial peptidoglycan-degrading enzymes and their impact on host muropeptide detection, J. Innate Immun. 1 (2009) 88–97, https://doi.org/10.1159/000181181.

[38] M. Eladawy, M. El-Mowafy, M.M.A. El-Sokkary, R. Barwa, Effects of lysozyme, proteinase K, and cephalosporins on biofilm formation by clinical isolates of Pseudomonas aeruginosa, Interdiscip. Perspect. Infect. Dis. 2020 (2020) 6156720, https://doi.org/10.1155/2020/6156720.

[39] D.J. Miller, P.A. Araujo, P.B. Correia, M.M. Ramsey, J.C. Kruithof, M.C.M.van Loosdrecht, B.D.Freeman, D.R.Paul, M. Whiteley, J.S.Vrouwenvelder, Short-term adhesion and long-term biofouling testing of polydopamine and poly(ethylene glycol) surface modifications of membranes and feed spacers for biofouling control, Water Research. 46 (12) (2012), 3737–3753. doi:https://doi.org/10.1016/j.watres.2012.03.058.

[40] H.C. Flemming, J. Wingender, The biofilm matrix, Nat. Rev. Microbiol. 8 (9) (2010) 623–633, https://doi.org/10.1038/nrmicro2415.